Norwegian University of Science and Technology

TFYXXXX Project thesis.

Diffraction study of Rochelle salt in the ferroelectric phase

December 22, 2012

Abstract

Abstract

Foreword

Short description of gathering of data.

Internship at ESRF

Starting project work september 2012

Acknowledgements

We would like to thank the following people for their help and input during the project:

- **Lars-Ivar Hesselberg Simonsen** for providing me with LaTeX templates and Makefile.

Contents

Chapter 1

Introduction

Very brief explanation of project.
Rochelle salt long history of study, but still unsolved problems
Motivation? What happens in the transition from para-electric to ferroelectric phase

Short breakdown of report content chapter for chapter

Chapter 2

The crystalline state

The crystalline state are ordered solids with a repeating structure in 3 dimensions. Structures on the nanomenter scale, and the way in which they are arranged determine many of the electric, mechanical and magnetic properties that we can observe on the macroscopic scale.

The basic unit of crystalline materials are often referred to as *the asymmetric unit*. By operating on this unit with a combination of symmetry axes one can obtain several equivalent representations oriented about a point in space. In nature symmetries generated this way are plentiful, such as the petals of a flower, the symmetric wings of a butterfly or the regular patterns on the sea urchin.

Using one or a combination of rotation- and inversion axes through a point one can express all symmetries about a point[8]. The inversion axes in contrast to pure rotations includes an inversion through some point on the axis. Collecting all the equivalent asymmetric units we form a basis which is repeated by translations to make up the crystal structure. The family of these operations can be deduced and described by point groups.

2.1 The point groups

The family of point groups enumerates all the operations which leaves the origin fixed, that is, non-translational symmetry. Rotations and inversion obviously satisfies this requirement. In principle any rotation about an axis is possible, but in crystals repetition in space is fundamental. It can be shown[8] that this requires rotational angles $\varphi = 2\pi/n$ where the fold number n is 1, 2, 3, 4 or 6. This *crystallographics restriction* means we only use a subset of the infinite number of point groups. This subset is dubbed the crystallographic point groups.

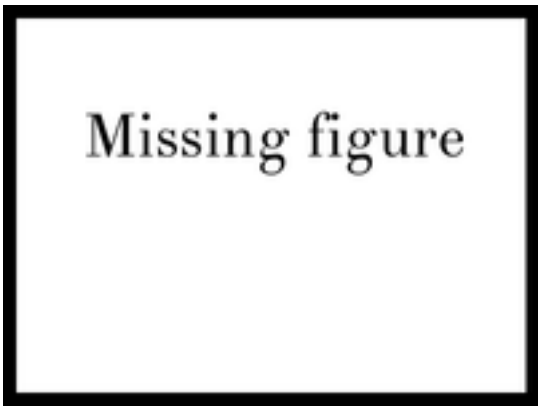

Figure 2.1: Demonstrating that $m \equiv \overline{2}$ — A twofold rotation followed by inversion through the origin. The rotation inverts the coordinates parallell to the mirroring plane while the inversion restores them leaving only the component normal to the plane.

In the notation of the International system it is usual to use mirror planes in addition to symmetry axes to describe point groups. Looking at figure 2.1 we see how a mirror plane, m, can be described by a two-fold axis $\overline{2}$ normal to the plane. The bar above the number denotes that the rotation is followed by inversion through the center, also called rotoinversion. Similarily, point groups with a centre of symmetry is equivalent to having an $\overline{1}$ axis.

The proper and improper rotations are represented by the symbols 1, 2, 3, 4, 6 and $\overline{1}$, $\overline{2}$, $\overline{3}$, $\overline{4}$, $\overline{6}$ respectively, whereas mirror planes are written as m. For combination of axes one writes $\frac{n}{m}$ for an n-fold rotation axis with a perpendicular mirror plane or nm for an n-fold rotation with a parallel mirror plane. The combination $\frac{n}{m}$ is equivalent to a rotation *and* an improper rotation $n \times \overline{n}$ about a common axis.

To derive the different point groups one has to combine symmetry axes in a systematic way. Defining two axes automaticly generates the third, so one can either have one symmetry axis n,$\overline{n}$,$n \times \overline{n}$ or a consistent set of three axes. For three axes there must be an even number of rotoinversion axes, i.e. they must be on the form RRR, RII, IRI or IIR. Finally, two rotations of same order must both be either R or I. A complete treatment[8] with these rules will lead to 32 unique point groups. They cover all the possible symmetries about one point in space and can be classified into 7 crystal systems as outlined in table 2.1 according to the order of its symmetry axes.

To realise the crystal the basis formed by the asymmetric unit must be repeated in space. We do this by assigning it to points in a lattice. The different arrangements of infinite, regular lattices were studied and correctly deduced by Bravais by the end of the 1840s [3].

Crystal system	A B C	Lattice systems
Triclinic	1 1 1	Triclinic
Monoclinic	1 2 1	Monoclinic
Orthorhombic	2 2 2	Orthorhombic
Trigonal	2 2 3	Rhombohedral, Hexagonal
Tetragonal	2 2 4	Tetragonal
Hexagonal	2 2 6	Hexagonal
Cubic	2 3 3 2 3 4	Cubic

Table 2.1: Crystal systems according to rotation order of symmetry axes A,B and C. Compatible lattice systems must include the same essential symmetry.

2.2 The Bravais lattices

The primitive Bravais lattices can be generated in three steps. First a primitive translation vector $\mathbf{a}$ is chosen and lattice points are repeated at a fixed period given by $\mathbf{a}$. If we allow the 1 dimensional line of points to repeat by another vector $\mathbf{b}$ which is not parallel to $\mathbf{a}$, we end up with a plane of lattice points. A third non-coplanar vector $\mathbf{c}$ fills the entire space with lattice points. There can be many choices for primitive vectors, but they are usually chosen to be as short as possible, and with highest possible symmetry, which allows one to express any lattice point by an integer number of translation operations. It is customary to define the set of primitive translation vectors $\mathbf{a}$, $\mathbf{b}$ and $\mathbf{c}$ in a right-handed system so that

$$|\mathbf{a}| = a,\ \angle(\mathbf{b},\mathbf{c}) = \alpha$$

$$|\mathbf{b}| = b,\ \angle(\mathbf{a},\mathbf{c}) = \beta$$

$$|\mathbf{c}| = c,\ \angle(\mathbf{a},\mathbf{b}) = \gamma.$$

Every lattice point can then be written as $\mathbf{R} = n_1\mathbf{a} + n_2\mathbf{b} + n_3\mathbf{c}$.

The volume spanned by a set of primitive translation vectors is referred to as *the primitive unit cell*. The magnitude of the volume is given by

$$V = |\mathbf{a} \cdot (\mathbf{b} \times \mathbf{c})|$$

Due to its infinite extent the Bravais lattices look the same at every point — they are invariant under translations expressed by $\mathbf{R}$. The set of translations to cover all lattice points in the lattice form a translation group. Bravais correctly classified these translation groups, or Bravais lattices into 14 lattice

Lattice system	Lengths	Angles
Triclinic	$a \neq b \neq c$	, $\alpha \neq \beta \neq \gamma$
Monoclinic	$a \neq b \neq c$	, $\alpha = \gamma = 90°, \beta \neq 90°$
Orthorhombic	$a \neq b \neq c$	, $\alpha = \beta = \gamma = 90°$
Tetragonal	$a = b \neq c$	, $\alpha = \beta = \gamma = 90°$
Rhombohedral	$a = b = c$	, $\alpha = \beta = \gamma \neq 90°$
Hexagonal	$a = b \neq c$	, $\alpha = \beta = 90°, \gamma = 120°$
Cubic	$a = b = c$	, $\alpha = \beta = \gamma = 90°$

Table 2.2: The lattice systems of Bravais lattices. Angles and lengths of **a**, **b** and **c** are given for their unit cells

Symbol	lattice points $(\mathbf{a}, \mathbf{b}, \mathbf{c})$
A—face	$(0, \frac{1}{2}b, \frac{1}{2}c)$
B—face	$(\frac{1}{2}a, 0, \frac{1}{2}c)$
C—face	$(\frac{1}{2}a, \frac{1}{2}b, 0)$
I	$(\frac{1}{2}a, \frac{1}{2}b, \frac{1}{2}c)$
F—face	$(0, \frac{1}{2}b, \frac{1}{2}c)$
	$(\frac{1}{2}a, 0, \frac{1}{2}c)$
	$(\frac{1}{2}a, \frac{1}{2}b, 0)$

Table 2.3: Coordinates of centered lattice points in non-primitive Bravais lattices. The primitive Bravais lattices are given the symbol P.

systems. Table 2.2 lists the different lengths and angles of their primitive translation vectors.

There are several ways of choosing unit cells, but one usually picks the ones which are more symmetric or closer to cubic. The primitive unit cells typically share one lattice point at each corner of the cell, so that the total number of lattice points in any cell is unity. For unit cells associated with the monoclinic, orthorhombic, tetragonal and cubic crystal systems the more symmetric unit cells can include 2, 3 or even 4 lattice points. An overview of these cells are given in figure 2.2. In this case the extra lattice points will *not* have integer coordinates, since they lie within or on the unit cell's faces. Table 2.3 lists the coordinates of centered lattice points.

Up till this point we have only considered the symmetyr of the unit cell in isolation. However, the repeating nature of the crystal allows new kinds of symmetry within the unit cells which are not from pure point operations. We can imagine a set of operations such that instead of returning to the original point in the unit cell one would end up at the equivalent point in a neighbouring unit cell. In this way order is still preserved in the crystal, and it is in fact a common feature of crystals. We will now see how this works for rotation axes and mirror planes.

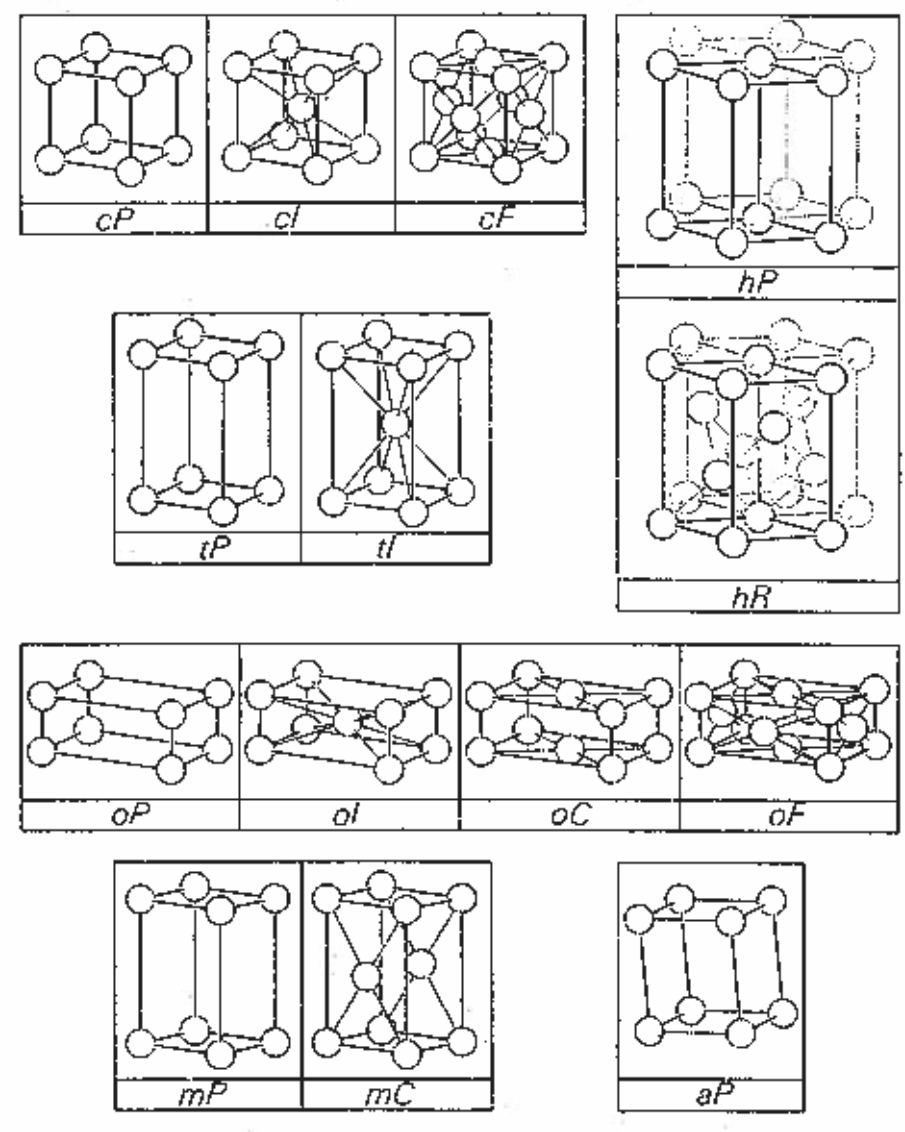

Figure 2.2: Depiction of the 7 lattice systems and 14 Bravais lattices using Pearson notation. The first letter assigns lattice systems cubic (c), trigonal (t), orthorhombic (o), monoclinic (m) and triclinic (a) — The rhombohedral lattice hR has been combined with the hexagonal lattice hP into a larger hexagonal family. The centering of the lattice is given by the second, capitalised letter as defined in table 2.3.

2.3 Screw axes

For rotation axes we can introduce a translation parallel to the axis; in this way the generated motifs looks the same when viewed along the axis. The screw axis operation then would be a combined rotation and translation. For an n-fold rotation axis there would be n rotations and translations within one period. If the axis is aligned along $\mathbf{a}$ one should translate a multiple of this distance after a full revolution

$$\mathbf{t} = \mathbf{a}\,\frac{m}{n}. \tag{2.1}$$

In addition to the rotation order n one must also specify the translation m to be applied as a subscript. For instance the screw axis 3_2 will do a three-fold rotation followed by a $\frac{2}{3}\mathbf{a}$ translation up the rotation axis as given by the right-hand rule. The available screw axes are 3_1; 4_1; 6_1; 6_2, their mirror images 3_2; 4_3; 6_4; 6_5 and 2_1; 4_2; 6_3 which have no handedness.

The screw axes look equivalent to rotational axes when looking at bulk symmetry, but result in some specific systematic absences in the diffraction patterns. The winding down the screw axis also makes the crystal optically active.

2.4 Glide planes

A glide plane is the combination of a mirror plane and translation. Points are mirrored and then translated parallel to the mirroring plane. The glide planes a,b and c involve one half translation along the respective axes while the n-glide is half a unit cell along two axial directions, a diagonal. More rarely a *diamond* glide plane can occur in which the translation is one fourth along two axial directions or for cubic and tetragonal system, the unit cell space diagonal.

With this we have covered the different symmetry elements available in crystals: point groups, space lattices, screw axes and glide planes. Combining all these operations leads to a full decsription of the symmetry of the crystal throughout space, the space groups.

2.5 Space groups

The space groups can be found by combining every possible symmetry of the unit cell with each Bravais lattice of same order. To generate all the possible

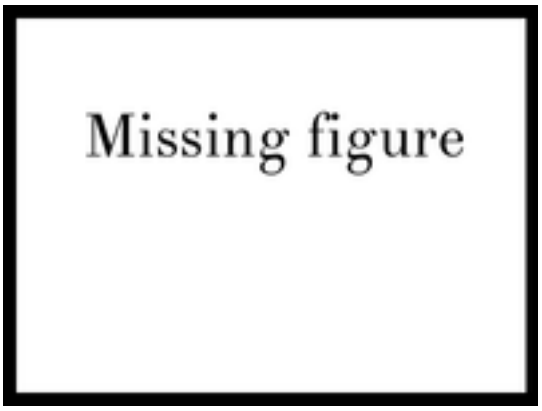

Figure 2.3: [10] (a) A unit cell with an a-glide plane. (b) The 2_1 screw axis operation. (c) 3_1 and 3_2 screw axes.

symmetries of the unit cell one systematically replaces rotation axes with screw axes and mirror planes with glide planes. This results in 230 distinct space groups as shown in table 2.4.

In the International system the notation of space groups starts with the centering of the Bravais lattice used[1] followed by high symmetry axes from the point group, or any screw axes and glide planes if present. The space group $P3_12$ for instance has no centering in the lattice, one 3_1 screw axis on the major axis and a 2 symmetry axis. Looking in table 2.1 we can deduce that the crystal system is trigonal.

[1] See table 2.3

Crystal system	Point groups	Space groups	Bravais lattices	Lattice system
Triclinic	2	2	1	Triclinic
Monoclinic	3	13	2	Monoclinic
Orthorhombic	3	59	4	Orthorhombic
Tetragonal	7	68	2	Tetragonal
Trigonal	5	7	1	Rhombohedral
		18	1	Hexagonal
Hexagonal	7	27		
Cubic	5	36	3	Cubic
7	32	230	14	7

Table 2.4: The distribution of space groups over Bravais lattices, point and space groups. Point groups and Bravais lattices are categorised into crystal and lattice systems respectively. The trigonal crystal system combines with both the rhombohedral and hexagonal lattice systems.

Chapter 3

X-ray Diffraction

- diffraction: the combined effect when waves are scattered and interfere with each other.

- common to all these fenomena is that significant effects only presents themselves when the wavelength of the wave is comparable to the repetition distance in the scattering geometry. Typical interatomic distance is of the order of 1Å with repeating units every 10Å or so.

In the following sections we will briefly deduce the scattering of X-rays by electrons leading to the diffraction from crystals. We will assume a *kinematical model* for the scattering with X-rays only interacting with weakly bound electrons.

Figures and presentation follows that of Woolfson[10] unless stated otherwise — We invite the reader to consult his chapter on scattering if more detail is required.

3.1 Scattering of X-rays

X-rays, due to their electromagnetic nature, interact most strongly with electons. In general we can think of the scattering interaction as an absorption followed by re-transmission in all directions[10]. The spatial distribution of energy of the scattered radiation depends on the specific scattering process, but there are many common features. We start by looking at the scattering of a wave from a single point in space, and progress to the scattering from a collection of points. Finally we consider the specific effects of electrons on X-ray scattering.

3.1.1 Scattering from single point

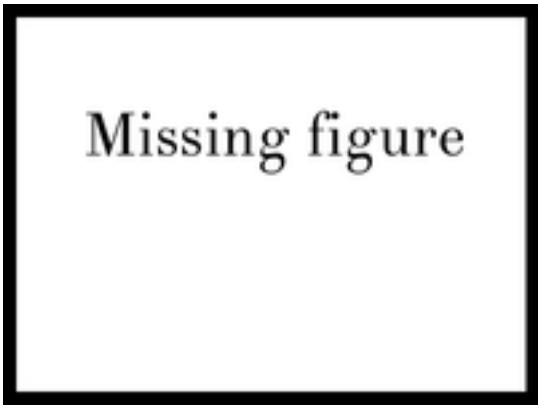

Figure 3.1: [10] Incident radiation scattered from point scatterer at O.

Consider the situation in figure 3.1. The incident radiation consists of a bundle of parallel, monochromatic rays propagating towards the scatterer at point O. The intensity at a point in the cylinder can be defined as the energy per unit time passing through a unit cross-section perpendicular to the direction of propagation.

At the point of the scatterer the power of the incident beam is scattered with a spherical distribution about O. The intensity is scattered over an ever-expanding sphere, so it will fall off as $\frac{1}{D^2}$ since the area covered goes as D^2. D is the distance OP in figure 3.1.

For interference we need to consider the displacements of the wave as it is being scattered. We define the displacement y_i of the monochromatic, incident wave at O as

$$y_i = A\cos(2\pi\nu t). \tag{3.1}$$

The frequency of the incident radiation is given by ν and its intensity I_0 is given by the square the displacement amplitude A. The displacement at point P will have the following modifications[10]:

1. Phase retardation $-2\pi D/\lambda$ due to traversing the distance $OP \equiv D$
2. *Scattering phase shift* α_s due to the scattering process at O.
3. Amplitude fall-off $1/D$ since intensity of scattered radiation falls of as $1/D^2$ and $I \sim A^2$.
4. The factor $f_{2\theta}$ dependent on scattering angle 2θ. This encapsulates the spatial distribution of the scattering process and is refered to as

the *scattering length* [10] due to its dimension.

Combined these factors give the following equation for the displacement at point P

$$y(2\theta, D, t) = f_{2\theta} \frac{A}{D} \cos(2\pi\nu(t - D/c) - \alpha_s) \tag{3.2}$$

where the relation $c = \nu \cdot \lambda$ has been used. It is more convenient to put 3.2 in complex form

$$y(2\theta, D, t) = f_{2\theta} \frac{A}{D} \exp(2\pi i\nu(t - D/c) - i\alpha_s) \tag{3.3}$$

where the real part still gives the displacement and their ratio (imaginary/real part) give the tangent of the phase difference from O. Let now the amplitude at P be denoted by

$$\eta(2\theta), D) = f_{2\theta} \frac{A}{D} \tag{3.4}$$

and the phase retardation

$$\alpha_{OP} = 2\pi\nu D/c + \alpha_s. \tag{3.5}$$

The intensity of the scattered radiation per unit solid angle is then given by

$$\begin{aligned} I_{2\theta} =& K[\eta(2\theta, D)]^2 \times D^2 = f_{2\theta}^2 K A^2 \\ I_{2\theta} =& f_{2\theta}^2 I_0 \end{aligned} \tag{3.6}$$

independent of distance D as requried by energy conservation.

3.1.2 Scattering from two points

Consider now two scatterers at points O_1 and O_2. In figure 3.2 they are shown joined by the vector $\mathbf{r}$ making some angle with the incident radiation $\hat{s}_0$. We want to find the displacement at P from the radiation scattered of O_1 and O_2. The distance $D \equiv O_1P$ to a detector should be much greater than the typical distance $|\mathbf{r}|$ between scatterers in a crystal, so the scattering angles from O_1 and O_2 are effectively identical.

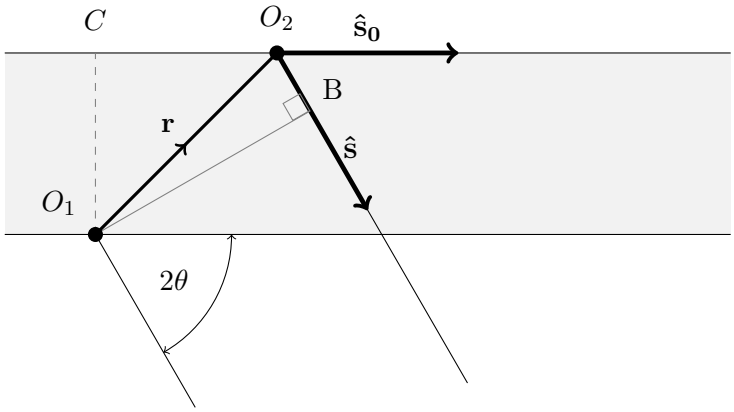

Figure 3.2: [10]Incident radiation on scatterers at O_1 and O_2. The scattered radiation converges to point P off-figure along $\hat{\mathbf{s}}$

If we also assume identical scatterers ($\alpha_{s_0} = \alpha_{s_1}$) the phase difference between the two paths is then

$$z\alpha_{O_1O_2} = \frac{-2\pi}{\lambda}(CO_2 + O_2B). \tag{3.7}$$

From the figure we see that

$$CO_2 = \mathbf{r} \cdot \hat{\mathbf{s}}_\mathbf{0} \quad , \quad O_2B = \mathbf{r} \cdot \hat{\mathbf{s}}. \tag{3.8}$$

So using only vectors

$$\alpha_{O_1O_2} = 2\pi\mathbf{r} \cdot (\hat{\mathbf{s}} - \hat{\mathbf{s}}_\mathbf{0}) \tag{3.9}$$

Let the *scattering vector* be given by

$$\mathbf{s} = \frac{\hat{\mathbf{s}} - \hat{\mathbf{s}}_\mathbf{0}}{\lambda}. \tag{3.10}$$

The phase difference 3.7 is then simply

$$\alpha_{O_1O_2} = 2\pi\mathbf{r} \cdot \mathbf{s}. \tag{3.11}$$

The simple geometry of the scattering vector can be seen in figure 3.3. The unit vectors are by definition of equal length. It follows that $\mathbf{s}$ is perpendicular to the line bisecting the scattering angle and hence its magnitude is given by

$$s = (2\sin\theta)/\lambda. \tag{3.12}$$

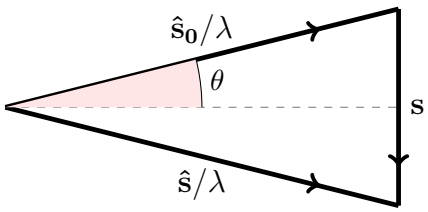

Figure 3.3: [10]The scattering vector and its relation to scattering angle 2θ.

If we let the incident displacement be described by 3.1 the displacement at P due to scattering at O_1 is still given by 3.3. The displacement at P is thus given by

$$\begin{aligned} y(2\theta, D, t) &= f_{2\theta}\frac{A}{D}\exp(2\pi i\nu(t - D/c) - i\alpha_s) \\ &+ f_{2\theta}\frac{A}{D}\exp(2\pi i\nu(t - D/c) - i\alpha_s + 2\pi i\mathbf{r}\cdot\mathbf{s}). \end{aligned}$$

and collecting common terms

$$y(2\theta, D, t) = f_{2\theta}\frac{A}{D}\exp(2\pi i\nu(t - D/c) - i\alpha_s)[1 + \exp(2\pi i\mathbf{r}\cdot\mathbf{s})]. \tag{3.13}$$

The combined amplitude becomes

$$\begin{aligned} \eta_2(2\theta, D) &= f_{2\theta}\frac{A}{D}\left[1 + \exp(2\pi i\mathbf{r}\cdot\mathbf{s})\right] \\ &= \eta(2\theta, D)[1 + \exp(2\pi i\mathbf{r}\cdot\mathbf{s})] \end{aligned} \tag{3.14}$$

where $\eta(2\theta, D)$ was the amplitude 3.4 we found for a single scatterer. This can be interpreted using a phase-vector diagram as in figure 3.4a where the vectors **AB** and **BC** have the same magnitude $\eta(2\theta, D)$ and their angle is the phase difference $2\pi\mathbf{r}\cdot\mathbf{s}$. The resultant amplitude **AC** has magnitude $\eta_2(2\theta, D)$ and phase difference given by angle ϕ with respect to radiation at O_1.

Here we have measured phases with respect to the scatterer at O_1, but we are free to measure the phase difference with respect to an arbitrary point O. This situation is shown in 3.4b where the two scatterers are given

coordinates r_1 and r_2 relative to some fixed scattering point O. Equation 3.14 then becomes

$$\eta_2(2\theta, D) = \eta(2\theta, D)[\exp(2\pi i \mathbf{r_1} \cdot \mathbf{s}) + \exp(2\pi i \mathbf{r_2} \cdot \mathbf{s})]. \tag{3.15}$$

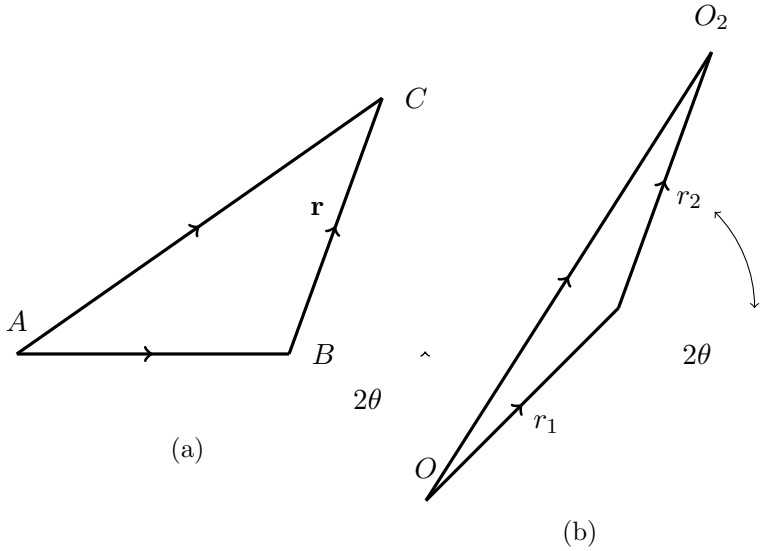

Figure 3.4: [10]Phase-vector diagram for two scatterers with (a) O_1 as origin and (b) O_1 at $\mathbf{r_1}$ and O_2 at $\mathbf{r_2}$.

3.1.3 Scattering from a collection of points

Having found the magnitude and phase of two scatterers relative to a point we are ready to generalize to a distribution of scattering points. Adding more scatterers to equation 3.15 we have

$$\eta_n(2\theta, D) = \sum_{j=1}^{n} \eta(2\theta, D) \exp(2\pi i \mathbf{r_j} \cdot \mathbf{s}). \tag{3.16}$$

For identical scatterers we can write the single amplitude outside the sum

$$\eta_n(2\theta, D) = \eta(2\theta, D) \sum_{j=1}^{n} \exp(2\pi i \mathbf{r_j} \cdot \mathbf{s}) \tag{3.17}$$

while in general for non-identical scatterers the scattering amplitudes $[\eta(2\theta, D)]_j$ must be taken inside the sum

$$\eta_n(2\theta, D) = \sum_{j=1}^{n} [\eta(2\theta, D)]_j \exp(2\pi i \mathbf{r_j} \cdot \mathbf{s})$$
$$= \frac{A}{D} \sum_{j=1}^{n} (f_{2\theta})_j \exp(2\pi i \mathbf{r_j} \cdot \mathbf{s}). \tag{3.18}$$

The *scattering lengths* of the different scatterers are now within the sum accounting for a general distribution of scatterers. We will now look closer at the mechanisms responsible for the different scattering lengths $f_{2\theta}$.

3.1.4 Coherent scattering

From classical electrodynamics[4] we know that x-rays are a form of electromagnetic radiation where harmonically accelerating electric and magnetic fields interact to propagate themselves in space. The basic interaction with electric charges can be summed up quite simply: Electric fields accelerate electric charges, and accelerating charges induces accelerating fields which themselves radiate energy in all directions.

J.J Thomson studied and formulated the theory of scattering of free (i.e. not bound or restrained) electrons and can be thought of as the absorption and re-emission of radiation in all directions. If the incident radiation is coherent and monochromatic we should expect a fixed phase relationship between incident and scattered radiation — the scattered radiation is coherent with respect to the incident radiation. For this system of free electrons the phase shift α_s is equal to π . The frequency, or wavelength of the radiation should obviously be the same as that associated with the oscillating electron.

Let us consider a harmonically oscillating electron at O as in figure 3.5, with mass m_e,charge e and acceleration amplitude a. The scattered radiation propagates along **OP** at an angle ϕ relative to the acceleration vector. The amplitude of the resulting electric field is given in [10] as

$$E = \frac{ea \sin(\phi)}{4\pi\varepsilon_0 r c^2} \tag{3.19}$$

at distance r perpendicular to **OP**.

In the next figure (3.6) we see the incident radiation decomposed into $E_\perp$ and $E_\parallel$ respectively perpendicular and parallel to the plane OXP. The acceleration experienced by an electron in these fields is

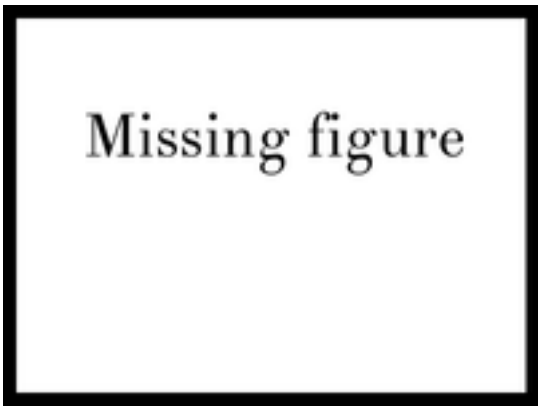

Figure 3.5: [10]The relationship of the electric vector for scattered radiation to the acceleration vector of an electron at O. Both vectors are in the plane of the page.

$$a_{\perp} = \frac{eE_{\perp}}{m_e}$$
$$a_{\parallel} = \frac{eE_{\parallel}}{m_e}. \tag{3.20}$$

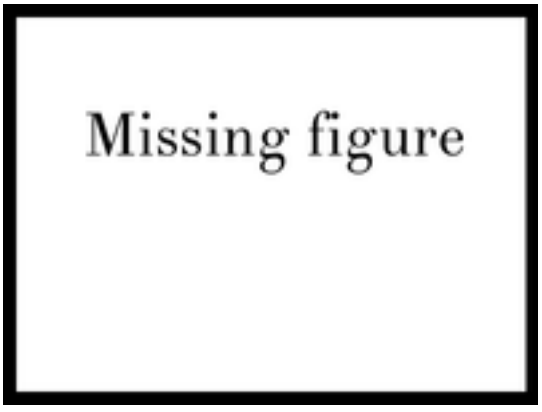

Figure 3.6: [10]The relationship of the electric vector for scattered radiation to the acceleration vector of an electron at O. Both vectors are in the plane of the page.

Applying the acceleration to equation 3.19 one finds the electric vector components

$$E'_\perp = (\frac{e^2}{4\pi\varepsilon_0 c^2 m_e})\frac{1}{r}E_\perp$$
$$E'_\parallel = (\frac{e^2}{4\pi\varepsilon_0 c^2 m_e})\frac{\cos(2\theta)}{r}E_\parallel \tag{3.21}$$

for the scattered wave at point P. The expression in parentheses is known in classical electrodynamics as the electron radius.

In equation 3.21 the electric field was calculated for a simple monochromatic wave polarized in some direction. Using the principle of superposition the response of arbitrary incident radiation can be found by summing up the contributions from their simple components.

In the case of unpolarized radiation we expect equal magnitudes averaged over time

$$\begin{aligned}\overline{|E_\perp^2|} = \overline{|E_\parallel^2|} &\propto \frac{1}{2}I_0 \\ &= \frac{1}{2}CI_0\end{aligned} \tag{3.22}$$

for some C where I_0 is the intensity of incident radiation. The intensity as power per unit solid angle at 2θ is then

$$\begin{aligned}I_{2\theta} &= \frac{1}{C}r^2(\overline{|E'_\perp|}^2 + \overline{|E'_\parallel|}^2) \\ &= \frac{1}{C}r^2(\frac{e^2}{4\pi\varepsilon_0 c^2 m_e})^2[1+\cos^2(2\theta)]\cdot\frac{1}{2}CI_0 \\ &= \frac{1}{2}r^2(\frac{e^2}{4\pi\varepsilon_0 c^2 m_e})^2[1+\cos^2(2\theta)]I_0.\end{aligned} \tag{3.23}$$

The factor $1/m_e^2$ shows clearly why the heavier protons aren't effective scatterers. To calculate the total power P scattered on an electron we use the relation

$$\begin{aligned}\mathrm{d}P &= I_\gamma \mathrm{d}\Omega \\ &= I_\gamma 2\pi\sin(\gamma)\mathrm{d}\gamma\end{aligned}$$

Using equation 3.23 and integrating over $\gamma = 0\ldots\pi$ one find the total power scattered by a single electron is

$$P = \frac{8\pi}{3}(\frac{e^2}{4\pi\varepsilon_0 c^2 m_e})^2 I_0. \tag{3.24}$$

For a material with n electrons per unit volume exposed to an incident beam of cross-sectional area β the total power scattered per unit path through the material is

$$P_l = P \cdot \beta n. \tag{3.25}$$

The ratio

$$\sigma = \frac{P_l}{\beta I_0} = \frac{nP}{I_0} = \frac{8\pi}{3}(\frac{e^2}{4\pi\varepsilon_0 c^2 m_e})^2 \tag{3.26}$$

of scattered power P_l to the power in the incident beam βI_0, is called the scattering power and is a measure of the fraction of incident radiation which is scattered per unit length. If one assumes as Woolfson[10] that all electrons in a material are free and a typical density 3×10^{29} electrons per m^{-2} $\sigma \approx 20$. Diffraction samples, which are typically thinner than 1 mm, will then scatter only 2% or less of the incident X-ray beam.

Experiments show that the majority of scattered radation is indeed coherent Thomson scattering, but a fraction of the scattered radation is found to have a longer wavelength compared to the incident radiation which is dependent on the scattering angle. This contribution can be described as the classical collision of a photon with the electron, coined compton scattering.

3.1.5 Compton scattering

We can imagine the process of compton scattering as a photon colliding elastically and imparting momentum to a free electron at rest. If the photon originally had an energy of $E = \frac{hc}{\lambda}$ conservation of energy requires that

$$\frac{hc}{\lambda} = \frac{hc}{\lambda + \mathrm{d}\lambda} + \frac{1}{2}m_e v^2 \tag{3.27}$$

where $\mathrm{d}\lambda$ is the change in wavelength for the photon and v is the resulting velocity of the recoiling electron. The first order approximation for small $\mathrm{d}\lambda$ is

$$\frac{hc}{\lambda^2}\mathrm{d}\lambda = \frac{1}{2}m_e v^2. \tag{3.28}$$

In addition linear momentum must be conserved. If the scattered photon forms an angle 2θ with the incident radiation the condition can be written[10] as

$$\frac{1}{2}m_e v = \frac{h}{\lambda}\sin\theta. \tag{3.29}$$

Combining equation 3.28 and 3.29

$$\mathrm{d}\lambda = \frac{h}{m_e c}\sin^2\theta$$

or

$$\mathrm{d}\lambda = \frac{h}{m_e c}(1-\cos 2\theta). \tag{3.30}$$

Replacing physical constants

$$\mathrm{d}\lambda = 0.024\text{Å}(1-\cos 2\theta). \tag{3.31}$$

Maximal change in wavelength is thus obtained for back-scattering photons ($2\theta = \pi$)

$$\mathrm{d}\lambda = 2\frac{h}{m_e c} \simeq 0.048\text{Å} \tag{3.32}$$

which while not very large, can be significant in comparison with X-rays having wavelengths around 1Å. Being incoherent the scattered compton radiation provides a background intensity as one sums up the incoherent radiation from different scatterers by their intensities and not their amplitudes ([10],p52).

Looking at thomson and compton scattering we treated incident radiation as waves and particles respectively. This is an example of the wave-particle duality of quantum mehcanics which we need in order to describe the scattering of electrons bound to an atom.

3.1.6 Scattering from an atom

The electrons in an atom are bound in discrete energy states. Compton scattering then, need to completely eject an outer electron or transfer it to another bound state, whereas thomson scattering must leave the electron in a state with same energy. A quantum mechanical treatment shows that the electron is not localised at any point but distributed about the atom. The electron is described by a complex function Ψ whose solution gives the charge distribution

$$\rho = |\Psi|^2 \tag{3.33}$$

in units of electron charge per unit volume. From this the coherent component can be found ([10],p47). Additionally the total scattered intensity due

to thomson and compton scattering is found to coincide with Thomson's formula 3.23.

To derive the amplitude of the coherently scattered radiation we start by considering the scattering amplitude for a collection of scatterers that we found in equation 3.18. Instead of considering discrete scattering points we now look at the contribution from a charge $\mathrm{d}q$ in the small volume element $\mathrm{d}V$. The equivalent integral should then be

$$\eta_{\mathbf{s}} = C_{\mathbf{s}} \int_{\mathrm{d}V} \mathrm{d}q \cdot \exp(2\pi i \mathbf{r} \cdot \mathbf{s}) \tag{3.34}$$

where C_{vecs} is some constant (possibly including the scattering vector $\mathbf{s}$) and $\mathbf{r}$ is the position of the volume element being integrated. The integral should cover all of space and shows that the resulting scattering is a standard fourier transform of the electron charge distribution.

If we assume that the electron charge density is symmetric about the origin we have in sperhical coordinates

$$\begin{aligned} & \mathrm{d}q = \rho(r)\ \mathrm{d}V \\ \text{or} \quad & \mathrm{d}q = \rho(r)\, r^2\ \mathrm{d}\Omega \\ & \quad = \rho(r)\, r^2 \sin(2\theta)\ \mathrm{d}\varphi\ \mathrm{d}(2\theta). \end{aligned} \tag{3.35}$$

Here 2θ is the same scattering angle as defined in previous sections, thus

$$\eta_{\mathbf{s}} = C_{\mathbf{s}} \int_{r=0}^{\infty} \int_{\theta=0}^{\pi} \int_{\varphi=0}^{2\pi} \rho(r) r^2\ \exp(2\pi i \mathbf{r} \cdot \mathbf{s}) \sin\theta\ \mathrm{d}\varphi\ \mathrm{d}\theta \tag{3.36}$$

and

$$\mathbf{r} \cdot \mathbf{s} = rs\cos(2\theta).$$

Since the distribution is assumed centro-symmetric we can write replace the exponential factor with cosine when integrating over the sphere[10] so

$$\eta_{\mathbf{s}} = C_{\mathbf{s}} \int_{r=0}^{\infty} \int_{\theta=0}^{\pi} \int_{\varphi=0}^{2\pi} \rho(r) r^2\ \cos(2\pi i \mathbf{r} \cdot \mathbf{s}) \sin\theta\ \mathrm{d}\varphi\ \mathrm{d}\theta \tag{3.37}$$

and integrating

$$\eta_{\mathbf{s}} = 4\pi\, C_{\mathbf{s}} \int_{r=0}^{\infty} \rho(r)\, r^2\ \frac{\sin(2\pi r s)}{2\pi r s} \mathrm{d}r. \tag{3.38}$$

Let us compare equation 3.38 with the scattering amplitude of an electron located at the origin. We write the electron density as $\rho(r) = \delta(r)$, where $\delta(r-a)$ is the dirac delta function centered at a. By definition[10]

$$4\pi \int_{r=0}^{\infty} r^2 \mathrm{d}r = 1 \qquad \text{and} \qquad \lim_{r\to 0} \frac{\sin(2\pi rs)}{2\pi rs} = 1. \tag{3.39}$$

Hence the reference amplitude is

$$(\eta_{\mathbf{s}})_0 = C_{\mathbf{s}}. \tag{3.40}$$

The ratio of scattered amplitude to that of an electron at the origin

$$p_s = 4\pi \int_{r=0}^{\infty} \rho(r)\, r^2\, \frac{\sin(2\pi rs)}{2\pi rs} \mathrm{d}r \tag{3.41}$$

is therefore only dependent on the magnitude of the scattering vector. For an atom with Z electrons the combined charge density would be $\rho_a(r) = \sum_j \rho_j(r)$. It follows that the atomic ratio of scattered coherent amplitude to that of a single electron at the origin is

$$f_a = \sum_j (p_s)_j. \tag{3.42}$$

The ratio f_a is referred to as the *atomic scattering factor*. The eletcron density in atoms can be approximated through a variety of methods for deriving the electron wave functions. The Hartree-Fock method, Thomas-Fermi model or Slater's analytical orbitals are but some of the existing ways of obtaining the radial electron density distribution $4\pi r^2\, \rho(r)$. The distribution for carbon as approximated by Slater's analytical wave functions is given in figure3.7 owing to Woolfson[10].

Looking at equation 3.41 we can still see some properties of the coherent scattering. The factor

$$\left\{ \frac{\sin(2\pi rs)}{2\pi rs} \right\} \to 1 \ , \text{ as } s \to 0$$

so the scattered radiation will be fully coherent in the forward ($\theta = 0$) direction. To see the intensity of the coherently scattered radiation by wave mechanics we square the atomic scattering factor and scale with the scattering intensity 3.23 Thomson found for a localized electron:

$$I_{Thomson} = (\sum_j (p_s)_j)^2 \times I_{2\theta}. \tag{3.43}$$

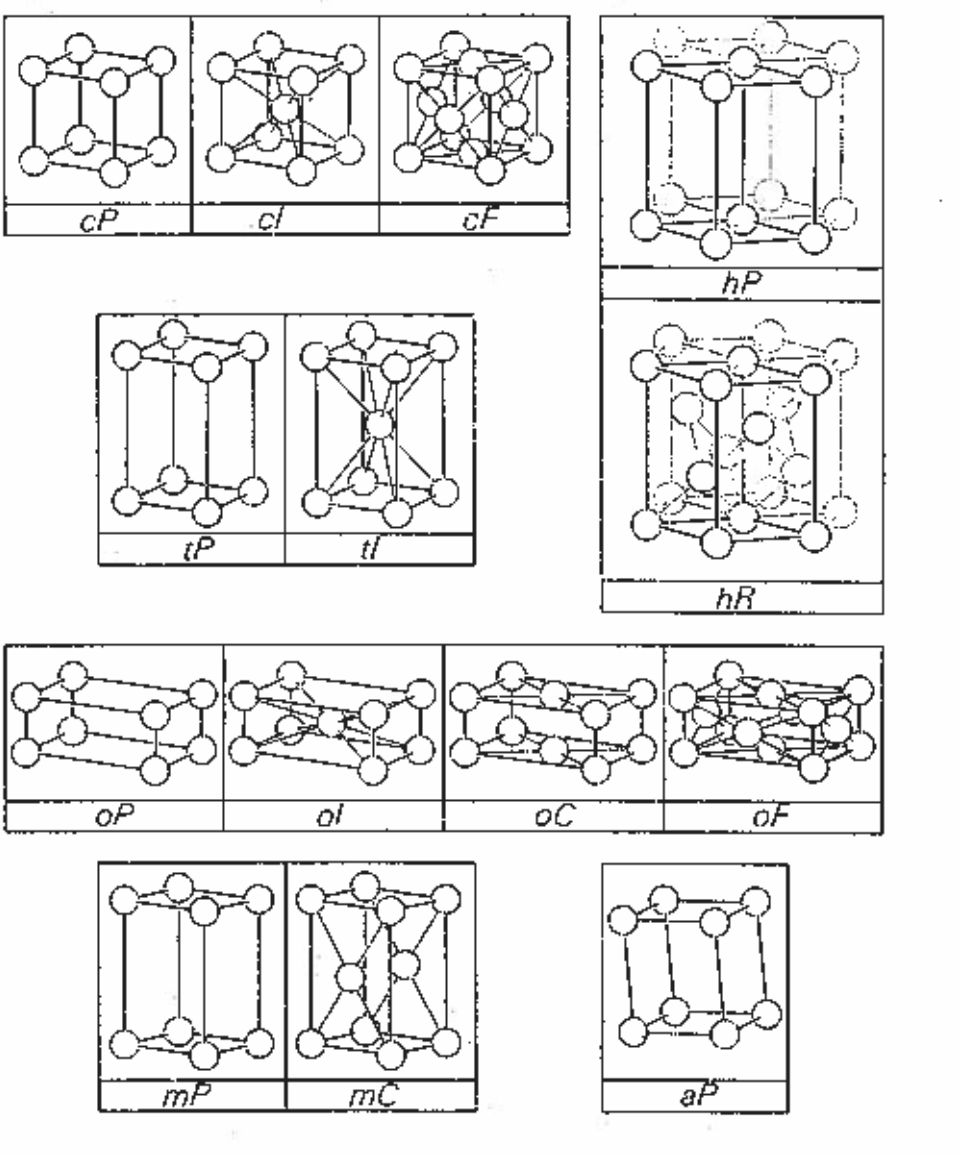

Figure 3.7: Radial electron density of Carbon.

In the previous section we noted that the Compton radiation is incoherent from one scatterer to another. The incoherent part is then the sum of the individual intensities $(1 - p_s^2)$

$$I_{Compton} = \sum_j (1 - (p_s)_j^2) \times I_{2\theta}. \tag{3.44}$$

When looking at the diffraction from a crystal there are contributions from a lot of scatterers, even in a thin sample. It should then be clear from equation 3.43 and 3.44 that the coherent contribution will dominate and incoherently scattered radiation will not be of great interest. For the coherent scattering, though, we want to look at the influence that the periodic nature of the scattering atoms have on the scattering amplitude.

3.2 Diffraction from a crystalline material

As discussed in chapter 2, crystalline materials consists of atoms in a three dimensional periodic pattern. In the last section we noted that the amplitude of a centrosymmetric distribution of scatterers will be real if the center is taken as the origin[10]. To start off we assume a single line with an odd number (n) of scatterers, defined by the translation vector $\mathbf{a}$. For a detector at a large distance compared to the extent of the line one finds the amplitude

$$A_n = f_a \sum_{q=-\frac{1}{2}(n-1)}^{\frac{1}{2}(n-1)} \cos(2\pi q \mathbf{a} \cdot \mathbf{s}) \tag{3.45}$$

where f_a is the atomic scattering factor from last section and the scattering vector $\mathbf{s}$ defines the scattering angle per equation 3.12. Again, the amplitude is relative to a point electron located at the origin which after some manipulation ([10],p54) can be written as

$$A_n = f_a \frac{\sin \pi n \mathbf{a} \cdot \mathbf{s}}{\sin \pi \mathbf{a} \cdot \mathbf{s}}. \tag{3.46}$$

The resulting intensity is

$$(A_n)^2 = f_a^2 \frac{\sin^2 \pi n \mathbf{a} \cdot \mathbf{s}}{\sin^2 \pi \mathbf{a} \cdot \mathbf{s}}. \tag{3.47}$$

The sine factor in equation 3.47 is very common when dealing with diffraction. It has main maximas whenever $\sin(\pi \mathbf{a} \cdot \mathbf{s}) = 0$, that is

$$\mathbf{a} \cdot \mathbf{s} = h \tag{3.48}$$

for some integer h. According to L'Hôpital's rule

$$\lim_{\mathbf{a}\cdot\mathbf{s}\to 0} \frac{\sin^2 \pi n\mathbf{a}\cdot\mathbf{s}}{\sin^2(\pi\mathbf{a}\cdot\mathbf{s})} = \frac{(n\mathbf{a}\cdot\mathbf{s})^2}{(\mathbf{a}\cdot\mathbf{s})^2} = n^2 \tag{3.49}$$

so the main peaks will necessarily have to become sharper as they grow with more scatterers. Between each main maxima there are $n-1$ minima and $n-2$ smaller maxima whose size depends on the magnitude of the denominator. This is easily seen if $\sin^2(\pi n\mathbf{a}\cdot\mathbf{s})$ and $\sin^2(\pi\mathbf{a}\cdot\mathbf{s})$ are plotted next to eachother.

In addition to the previous properties Woolfson[10] notes that the ratio of main maximas to the secondary maximas increases with n. As we mentioned in the introduction of this chapter a crystal will typically have unit cells repeated every 10Å which equates to 10^6 cells per mm. Except for very small samples the diffraction intensity will therefore consist of narrow peaks at the positions given by equation 3.48.

Crystal diffraction is readily generalized to 2 and 3 dimensions. If we follow the convention of the Bravais lattices from section 2.2 each line of scatterers will repeat itself along the translation vectors $\mathbf{b}$ and $\mathbf{c}$ in three dimensions. The diffraction condition can be decomposed into the three equations

$$\begin{aligned} \mathbf{a}\cdot\mathbf{s} &= h \\ \mathbf{b}\cdot\mathbf{s} &= k \\ \mathbf{c}\cdot\mathbf{s} &= l \end{aligned} \tag{3.50}$$

collectively known as the *Laue equations*. Since there is now a direct relationship between the scattering vector $\mathbf{s}$ and the primitive lattice vectors we can attempt to find a basis for the scattering vectors $\mathbf{s}_{hkl}$ satisfying 3.50.

3.2.1 The reciprocal lattice

We start by assuming that we can find a basis $\{\mathbf{a}^*, \mathbf{b}^*, \mathbf{c}^*\}$ so that $\mathbf{s}_{hkl}$ can be written on the form

$$\mathbf{s}_{hkl} = h\mathbf{a}^* + k\mathbf{b}^* + l\mathbf{c}^*. \tag{3.51}$$

Using matrix notation equation 3.50 take the form

$$\begin{bmatrix} \mathbf{a} \\ \mathbf{b} \\ \mathbf{c} \end{bmatrix} \mathbf{s} = \begin{bmatrix} h \\ k \\ l \end{bmatrix} \tag{3.52}$$

and inserting for $\mathbf{s}_{hkl}$

$$\begin{bmatrix} \mathbf{a} \\ \mathbf{b} \\ \mathbf{c} \end{bmatrix} \begin{bmatrix} \mathbf{a}^* & \mathbf{b}^* & \mathbf{c}^* \end{bmatrix} \begin{bmatrix} h \\ k \\ l \end{bmatrix} = \begin{bmatrix} h \\ k \\ l \end{bmatrix}$$

or

$$\begin{bmatrix} \mathbf{a}\mathbf{a}^* & \mathbf{a}\mathbf{b}^* & \mathbf{a}\mathbf{c}^* \\ \mathbf{b}\mathbf{a}^* & \mathbf{b}\mathbf{b}^* & \mathbf{b}\mathbf{c}^* \\ \mathbf{c}\mathbf{a}^* & \mathbf{c}\mathbf{b}^* & \mathbf{c}\mathbf{c}^* \end{bmatrix} \begin{bmatrix} h \\ k \\ l \end{bmatrix} = \begin{bmatrix} h \\ k \\ l \end{bmatrix}. \tag{3.53}$$

Since this must hold for all hkl we have $\{\mathbf{a}^*, \mathbf{b}^*, \mathbf{c}^*\}$ defined by the set of equations

$$\begin{array}{lll} \mathbf{a}\mathbf{a}^* = 1, & \mathbf{a}\mathbf{b}^* = 0, & \mathbf{a}\mathbf{c}^* = 0 \\ \mathbf{b}\mathbf{b}^* = 0, & \mathbf{b}\mathbf{b}^* = 1, & \mathbf{b}\mathbf{c}^* = 0 \\ \mathbf{c}\mathbf{a}^* = 0, & \mathbf{c}\mathbf{b}^* = 0, & \mathbf{c}\mathbf{c}^* = 1. \end{array} \tag{3.54}$$

Just like the primitive translation vectors $\{\mathbf{a}, \mathbf{b}, \mathbf{c}\}$ defined a lattice for the crystal's unit cells so $\{\mathbf{a}^*, \mathbf{b}^*, \mathbf{c}^*\}$ defines a lattice in *reciprocal space* for the allowed scattering vectors. It is called reciprocal since, as we see from the relation $\mathbf{a}\mathbf{a}^* = 1$, larger distances in the space of the crystal must correspond to smaller distances in the space of scattering. It can be shown that the set 3.54 leads to the definitions

$$\mathbf{a}^* = \frac{\mathbf{b} \times \mathbf{c}}{\mathbf{a} \cdot (\mathbf{b} \times \mathbf{c})}, \qquad \mathbf{b}^* = \frac{\mathbf{c} \times \mathbf{a}}{\mathbf{b} \cdot (\mathbf{c} \times \mathbf{a})}, \qquad \mathbf{c}^* = \frac{\mathbf{a} \times \mathbf{b}}{\mathbf{c} \cdot (\mathbf{a} \times \mathbf{b})} \tag{3.55}$$

which is uniquely defined for a given lattice $\{\mathbf{a}, \mathbf{b}, \mathbf{c}\}$. Having found that the diffraction peaks lies on a lattice it is time to see which reflections will be active for a particular orientation of the crystal.

3.2.2 Construction of the Ewald sphere

The Ewald sphere is a way of visualising the scattering vectors in the reciprocal lattice. The trivial scattering vector $s = 0$ corresponding to the primary incident ray always satisfies the laue equations. This means we can always draw the incident radiation vector $\hat{\mathbf{s}}_\mathbf{0}/\lambda$ so that it ends in the origin O originating from some point S in the reciprocal lattice, as we have done in figure 3.8.

The vector $\hat{\mathbf{s}}/\lambda$ is of same length and originating at the same point S it defines a sphere of possible scattering directions. In the figure only point H simultaneously satisfies the laue equations 3.50 in the plane $\mathbf{c}^* = 0$ – That is, only reflections corresponding to lattice points intersecting the Ewald sphere will be active for a particular crystal orientation. We recognize the scattering diagram 3.3 as the triangle $\triangle OSH$. If we imagine the crystal to

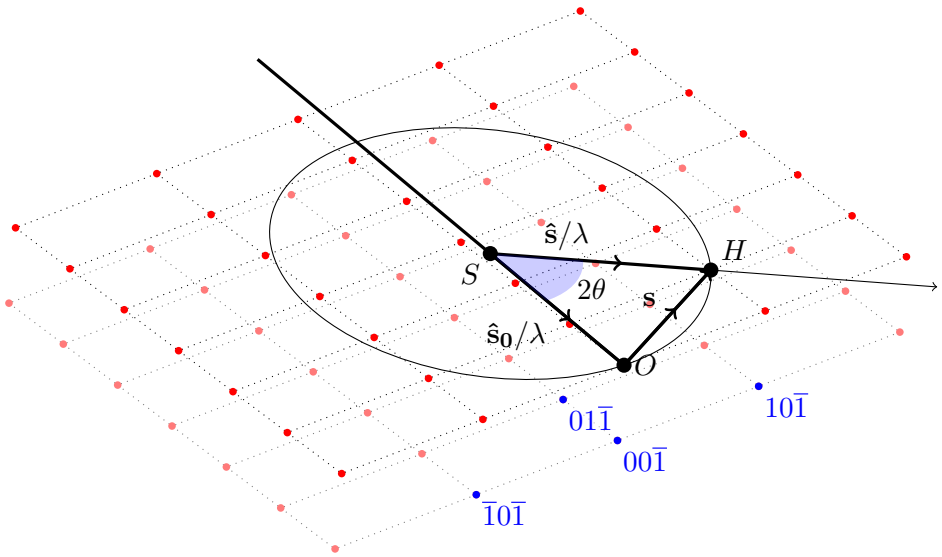

Figure 3.8: Construction of Ewald's sphere in the reciprocal lattice. The crystal is imagined to lie in the center S of a sphere of radius $1/\lambda$ which tangents the origin 000 of the reciprocal lattice. Diffraction occurs whenever a lattice point H intersects the sphere; The scattering angle relative to the incident radiation $\hat{\mathbf{s}}_\mathbf{0}$ is 2θ.

lie at the center S of Ewald's sphere and extend $\hat{\mathbf{s}}_\mathbf{0}$ and $\hat{\mathbf{s}}$, the the physical interpretation is easily seen: Incident radiation enters the crystal and exits at an angle 2θ towards the lattice point of that particular reflection, hopefully to be captured somewhere in the experimental setup.

For monochromatic X-rays and perfect crystals the Ewald sphere and reciprocal lattice is sharply defined and so there is seldom more than one reflection active at any configuration. However if the crystal is rotated, the reciprocal lattice rotates with it and other reciprocal lattice points may intersect the Ewald sphere and diffract. For some orientations more than one reflection might occur. This is called *multiple scattering* and can in some cases lead to diffraction for an index hkl even though $F(hkl) = 0$[1]. Note that for any diffraction to occur the Ewald sphere must have a radius at least as large as the magnitude of one of the reciprocal lattice vectors $\{\mathbf{a}^*, \mathbf{b}^*, \mathbf{c}^*\}$.

3.2.3 Covering the reciprocal lattice

For transmission electron microscopy and γ-rays the large size of the ewald sphere relative to the reciprocal lattice spacing means that the curvature of the sphere can become neglegible and multiple scattering becomes the norm rather than the exception with several reflections showing at the same

time. Other methods[1] for covering the reciprocal lattice includes the Laue method, the Debye-Scherrer method and a collection of methods for rotating and oscillating the sample.

The Laue method consists of using polychromatic or "white" radiation to cover a larger part of the reciprocal lattice simultaneously. If the radiation is in the range $(1/\lambda_{max} - 1/\lambda_{min})$ we can visualise the diffracting lattice points as those who fall within the Ewald sphere of radius $1/\lambda_{min}$ but outside the sphere with radius $1/\lambda_{max}$. Using the intense, polychromatic radiation from a third generation synchrotron it is possible to gather on the order of 1000 reflections in a single bunch of electrons ([1],p162) enabling high temporal resolution.

In place of changing the area spanned by the Ewald sphere one can irradite an ensemble of small crystalls, or crystalites, of different orientation. The Ewald sphere will then contain a superposition of reciprocal lattice points at different orientations. This is called powder diffraction and, if the crystalites are distributed randomly, it is characterised by continuous rings in the diffraction pattern from Debye-Scherrer cones formed by each index hkl.

Finally, direct manipulation of the crystal itself will also rotate the reciprocal lattice. By scanning or oscillating through an angle it is therefore possible to bring new lattice points to the surface of the Ewald sphere for diffraction. Care must be taken when designing a diffraction experiment, though, to ensure that a sufficient number of unique reflections are included for data analysis. It follows from the symmetries of the assymetric unit in the unit cell of chapter 2 that there will be some degree of redundant information, or symmetry, in the reciprocal lattice as well. In the absence of *anamalous scattering* and neglegible absorption the diffraction patterns are all centrosymmetric and are grouped into Laue classes corresponding to the 11 centrosymmetric point groups.

3.3 The structure factor

So far we considered the coherent scattering of eletcrons bound to atoms in a lattice. In a final step we will now consider the effect on scattering amplitude by the arrangement of atoms in the unit cell. If we follow the same reasoning as in deriving the atomic scattering factor from equation 3.18 we are led to the expression

$$F_{cell}(s) = \sum_j (f_a)_j \exp(2\pi i \mathbf{r}_j \cdot \mathbf{s}) \tag{3.56}$$

where we sum over all atoms j with scattering factor $(f_a)_j$ and position $\mathbf{r}_j$ relative to the center of the unit cell. The atoms include the asymmetric unit and all its equivalent representations as described in chapter 2.

If we express $\mathbf{r}$ and $\mathbf{s}$ as fractional coordinates in the lattices $\{\mathbf{a}, \mathbf{b}, \mathbf{c}\}$ and $\{\mathbf{a}^*, \mathbf{b}^*, \mathbf{c}^*\}$

$$F_{cell}(s) = \sum_j (f_a)_j \exp(2\pi i (x\mathbf{a}, y\mathbf{b}, z\mathbf{c}) \cdot (h\mathbf{a}^*, k\mathbf{b}^*, l\mathbf{c}^*)). \tag{3.57}$$

and apply the relations 3.50 we end up with the convenient form

$$F_{cell}(hkl) = \sum_j (f_a)_j \exp(2\pi(xh + yk + zl)). \tag{3.58}$$

Just as the atomic scattering factor was the fourier transform of the electron charge distribution about the nucleus we find that the scattering factor, known as the *structure factor*, of the unit cell is the fourier transform of the distribution $\rho_{cell}(r)$ over the unit cell. Since the crystal is generated by repeating the unit cell along $\{\mathbf{a}, \mathbf{b}, \mathbf{c}\}$ we can write the density for an infinite crystal as

$$\rho_\infty(\mathbf{r}) = \rho_{cell}(r) \star \sum_{u,v,w=-\infty}^{\infty} \delta(\mathbf{r} - \mathbf{r}_{uvw}). \tag{3.59}$$

Convolution with $\delta(\mathbf{r} - \mathbf{a})$ is equivalent with shitfting the function's origin to $\mathbf{a}$, so each term in the sum corresponds to one instance of the unit cell in the crystal. Using the fact that $\mathcal{F}\{\rho_{cell}\} = F_{cell}$ we can perform the fourier transform of 3.59 as

$$F_\infty(\mathbf{s}) = \frac{1}{V} F_{cell}(\mathbf{s}) \sum_{h,k,l} \delta(\mathbf{s} - \mathbf{s}_{hkl}) \tag{3.60}$$

where we have emphasized the fact that diffraction only occurs at the reciprocal lattice points $\{h, k, l\}$ on the Ewald sphere in figure 3.8. Equation **??** shows that it is in theory sufficient to find the structure factors for the different reflections $\{h, k, l\}$ if one wants to derive the structure of the crystal.

In practice real crystals have some factors affecting their structure factors:

1. "Ringing effects" due to finite crystal size. This has the effect of broadening the diffraction peaks making it necessary to scan about the peak in reciprocal space to record the full contribution.
2. Truncation of the fourier coefficients due to missing reflections. For higher scattering angles this effect is luckily small since the atomic scattering factors fall off pretty quickly (see figure 3.7).
3. Anamalous dispersion of radiation close to absorption edges.

The most significant factor though, is the acquisition of the scattered radiation istelf. Films, CCDs and other imaging devices record only intensities so the phase of the structure factors are not retained. Moreover, quantum mechanic fundamentals prohibit any complete measurement to be made. This is referred to as the *crystallographic problem*. We will explain briefly in section **??** how the phases

$$\phi_{hkl} = \frac{\Im\mathrm{m}(F(hkl))}{\Re\mathrm{e}(F(hkl))} \tag{3.61}$$

can be at least partially reconstructed from the measured intensities $I \propto |F_o(hkl)|^2$.

The reflection intensities are usually measured over long periods of time and for crystals spanning a large number of unit cells. The computed structure factors will therefore be some spatial and temporal average of the atoms displacement. Some factors[9] displacing atoms from the position in an imagined perfect crystal are

1. different energetically ecquivalent positions for atoms in unit cells ("static disorder")
2. transitions between energetically ecquivalent positions in the unit cell itself ("dyanimc disorder")
3. thermal vibration of atoms
4. lattice defects and vibrations

which all tend to attenuate the coherent diffraction peaks. The combined effect of these factors are usually captured in the temperature factor due to Peter Debye and Ivar Waller in a first approximation.

3.3.1 The temperature factor

The equation given for the structure factor was

$$F(\mathbf{s}) = \frac{1}{V}\sum_j (f_a)_j \exp(2\pi i \mathbf{r}_j \cdot \mathbf{s} \tag{3.62}$$

We now allow the atoms to vibrate by introducing a stochastic variable $\mathbf{u}$ to the atom position

$$\mathbf{r}_j = <\mathbf{r}> + \mathbf{u} \tag{3.63}$$

where $<\mathbf{r}>$ is the time average or mean position of the atom and $<\mathbf{u}>= 0$. It can be shown[1] that this perturbation leads to two distinct terms for the averaged intensities. The first term is coherent as usual and falls off exponentially with the mean squared displacement $< u^2 >$, while the other *increases* with $< u^2 >$ and depends on the correlation $< u_m u_n >$ between the displacements of atoms. This is found as a diffuse background in the vicinity of the diffraction peaks and is called *thermal diffuse scattering*.

The coherent term can be expressed as a modified atomic scattering factor

$$f_a \rightarrow f_a \exp(-2\pi^2 |s|^2 < u^2 >). \tag{3.64}$$

Using equation 3.12

$$f_a \rightarrow f_a \exp(-8\pi^2 \frac{\sin^2(\theta)}{\lambda} < u^2 >) \tag{3.65}$$

where the factor $8\pi^2 < u^2 >$ is known by the symbol B as the temperature factor. Contrary to what one might intuitively think the width of the diffraction peaks remain unchanged by the temperature factor. The temperature factor is usually expressed as a isotropic, gaussian distribution over the atom position, or if enough data is available as an anisotropic trivariate gaussian distribution. In the latter case the stochastic variable $\mathbf{u}$ can be described by its covariance matrix

$$[U_{ij}] = \begin{bmatrix} U_{11} & U_{12} & U_{13} \\ U_{12} & U_{22} & U_{23} \\ U_{13} & U_{23} & U_{33} \end{bmatrix} \tag{3.66}$$

relative to the reciprocal lattice vectors and the electron density of the atom can be viewed as ellipsoids. Unfortunately a number of conventions for

specifying these anisotropic displacements are used — Fortunately Grosse-Kunstleve and Adams[5] have compiled a summary of those commonly encountered when dealing with refinement software.

Chapter 4

Sources of radiation

Types of radiation use din diffraction experiments.
About the properties, production and application of
Elements of Modern X-ray Physics[2]

4.1 X-rays

4.1.1 x-ray tube

4.1.2 synchrotron

4.2 Neutrons

Notes given by Guorong Li [7]
Reactor. Thermal neutrons typical wavelength compared to atomic cross-section

4.3 Electrons

Chapter 5

Ferroelectricity

5.1 A brief history of ferroelecricity

Evolved into an important field in condensed matter physics paving way for innovations such as ...

5.2 Rochelle salt

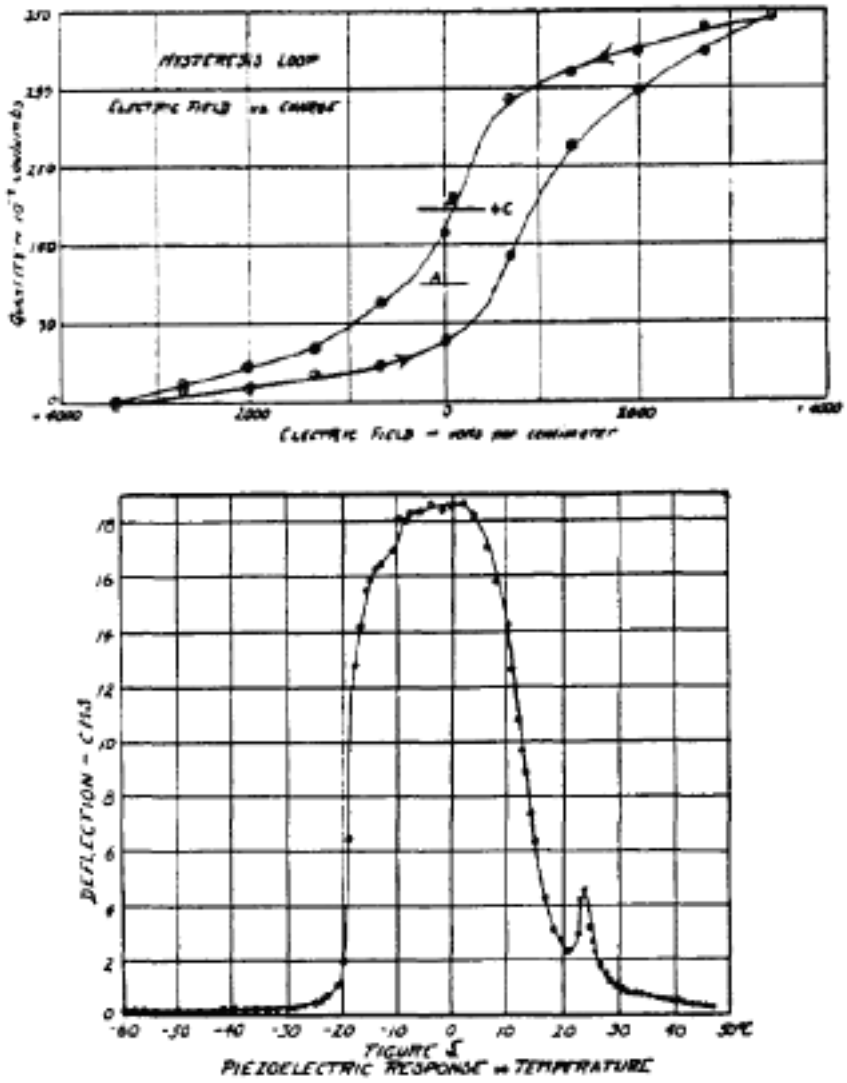
HYSTERESIS LOOP
ELECTRIC FIELD vs CHARGE
+C
-C
DEFLECTION - CMS
FIGURE 5
PIEZOELECTRIC RESPONSE vs TEMPERATURE

Figure 5.1

Chapter 6

Data Analysis

6.1 Correction of diffraction data

Which aberrations are left after optics hutch?
Ununiformity resulting from Xray optics (vignetting++), beam-properties etc

6.1.1 Dark current subtraction

6.1.2 Flat field

6.1.3 Sample absorption

correction due to different absorption in sample for different angles of scattering planes
Lorentz factor, polarization factor?

6.2 Crystal solution

6.2.1 Direct methods

6.2.2 Patherson method

6.3 Crystal refinement

Hammond[6]?

Placement of heavy atoms -¿ other atoms -¿ anisotropy -¿ disorder -¿ h atoms

6.3.1 Least squares optimization

Reconstructing density and run optimization against known intensities

6.3.2 Averaging of structur factors

6.3.3 Disorder

Static disorder

Dynaimc disorder

6.3.4 Refinemet statistics

Statistical criterions for solution fitness / residuals *including* accepted ranges with references

See comments p19 of Nielsen's project

$$\omega R = \sum \omega_o^2 - F_c^2 \tag{6.1}$$

Chapter 7

Experiment

7.1 Equipment

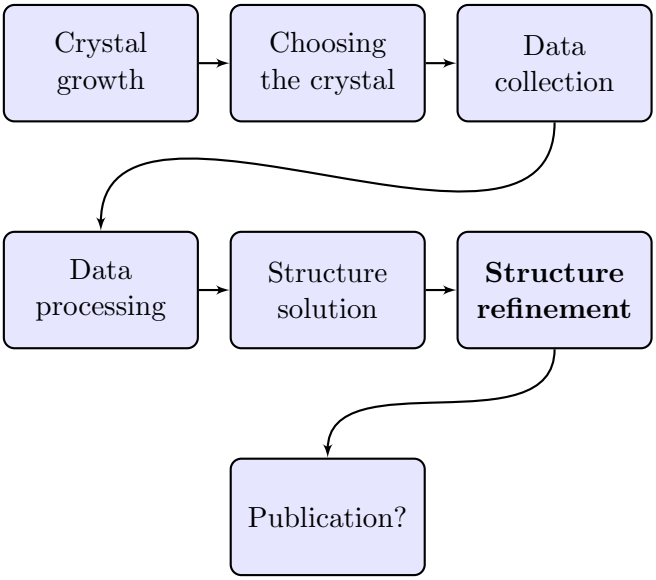

Figure 7.1: Flow of an X-ray diffraction study from crystal growth to publication. Structure refinement has been highlighted since this has been the subject of the project thesis.

Setup at the ESRF

7.2 Procedure

Mode of acquisition?

Software used to perform corrections. Refer to appendix

Lorentz-polarization factor. Sample absorption.

Chapter 8

Results

We'll see about this chapter

8.1 Crystal solution

Already determined? Cite reference

8.2 Data reduction

Correct laue group? Comment on systematic extinctions consistent with space group

8.3 Refinement

Chapter 9

Discussion

Was cake good or too good?

Chapter 10

Conclusion and Further Work

Cake was good.

Appendices

Appendix A

Test

Append everything to the cake!

Bibliography

[1] Jens Als-Nielsen and Des McMorrow. *Kinematical scattering II: crystalline order*, pages 147–205. John Wiley & Sons, Inc., 2011.

[2] Jens Als-Nielsen and Des McMorrow. *sources*, pages 29–67. John Wiley & Sons, Inc., 2011.

[3] A. Bravais and A.J. Shaler. *On the systems formed by points regularly distributed on a plane or in space*. Number 1. Crystallographic Society of America, 1949.

[4] D.J. Griffiths and Reed College. *Introduction to electrodynamics*. Pearson, 3 edition, 2008.

[5] R.W. Grosse-Kunstleve and P.D. Adams. On the handling of atomic anisotropic displacement parameters. *Journal of applied crystallography*, 35(4):477–480, 2002.

[6] Christopher Hammond. *The Basics of Crystallography and Diffraction*. Oxford University press, third edition, 2009.

[7] Guorong Li. Introduction to neutron scattering. Accessed 2012-10-22 22:40, 2008.

[8] Frode Mo. Crystallography. Lecture notes, 2002.

[9] T.R. Schneider. What can we learn from anisotropic temperature factors. *Proceedings of the CCP4 Study Weekend (Dodson, E., Moore, M., Ralph, A. & Bailey, S., eds)*, pages 133–144, 1996.

[10] M. M. Woolfson. *An Introduction to X-ray Crystallography*. Cambridge University press, 1970.